NANO LETTERS

2009
Vol. 9, No. 7
2742-2746

Photonic Crystal Geometry for Organic Solar Cells

Doo-Hyun Ko,[†] John R. Tumbleston,[‡] Lei Zhang,[†] Stuart Williams,[†] Joseph M. DeSimone,[†] Rene Lopez,[‡] and Edward T. Samulski*[,†]

Department of Chemistry, University of North Carolina at Chapel Hill, Caudill and Kenan Laboratories CB 3290, Chapel Hill, NC, and Department of Physics and Astronomy, University of North Carolina at Chapel Hill, Phillips Hall CB 3255, Chapel Hill, NC

Received April 17, 2009; Revised Manuscript Received May 21, 2009

ABSTRACT

We report organic solar cells with a photonic crystal nanostructure embossed in the photoactive bulk heterojunction layer, a topography that exhibits a 3-fold enhancement of the absorption in specific regions of the solar spectrum in part through multiple excitation resonances. The photonic crystal geometry is fabricated using a materials-agnostic process called PRINT wherein highly ordered arrays of nanoscale features are readily made in a single processing step over wide areas (~4 cm^2) that is scalable. We show efficiency improvements of ~70% that result not only from greater absorption, but also from electrical enhancements. The methodology is generally applicable to organic solar cells and the experimental findings reported in our manuscript corroborate theoretical expectations.

Incommensurate length scales conspire to degrade photovoltaic efficiencies in organic solar cells. Exciton diffusion lengths (~10 nm) are an order of magnitude smaller than absorption lengths.[1,2] This discrepancy is ameliorated by coprecipitating a bicontinuous donor and acceptor phase, a disordered bulk heterojunction (BHJ),[1,3] but inherent disadvantages persist: low exciton dissociation probability,[4] mismatched band gaps,[5] and optical losses.[6] Optimized BHJ devices have active layer thicknesses of ~100 nm due to the device-limiting trade-off between optical absorption and electrical performance.[7,8] These thicknesses are adequate to absorb most photons in the visible range of the solar spectrum due to the strong extinction coefficient of contemporary BHJ materials.[2,9] However, the sun's maximum photon flux is located around $\lambda = 700$ nm, which is near the band edge of many BHJ materials where absorption is weak. Energy-level engineering via custom synthesis[5] has produced so-called low-bandgap polymers[10] that exhibit broader absorption tails but are located further toward the near-infrared. The active layer thickness constraints imposed on BHJ solar cells make it imperative to develop innovative ways to enhance absorption in a specific spectral range with weak absorption without increasing photoactive layer thickness.

Light trapping schemes based on ray optics have provided enhancement in optical absorption, e.g. collector mirrors,[11] microprism substrates,[12] and V-folded configurations,[13] but in these schemes absorption enhancement was not tailored to a desired spectral range. Methods based on wave optics have shown greater promise, and both diffraction gratings[14−16] and photonic crystal (PC) designs have been investigated. In particular, theoretical considerations of PC geometries suggest efficiency improvements would be anticipated[17−19] for organic solar cells similar to theoretical work on inorganic devices.[20,21] In spite of this theoretical promise, there has been little progress in experimentally demonstrating PC effects in organic solar cells. While there has been success in nanopatterning the photoactive layer, the primary intention has been to provide an undulating surface for evaporating a metal diffraction grating[14,22,23] or to make an ordered BHJ device.[24] Herein, we report a two-dimensional periodic PC organic solar cell made from highly ordered arrays of columnar features. The PC is readily fabricated via Pattern Replication In Nonwetting Templates (PRINT),[25] a materials-agnostic process that lends itself to large area replication of nanoscale features. As a proof of concept, we use a BHJ blend of the thermally deprotectable polythiophene derivative (TDPTD) poly(3-(2-methyl-2-hexyl-carboxylate) thiophene-co-thiophene)[26] and [6,6]-phenyl-C_{61}-butyric acid methyl ester (PCBM), but the fabrication method could be applied to any photoactive polymer processed from solution.

We demonstrate 3-fold absorption enhancements near the band edge of TDPTD:PCBM due to a PC geometry. We show efficiency improvements of ~70% that result not only from improved absorption, but also from intriguing electrical

* To whom correspondence should be addressed. E-mail: et@unc.edu.
[†] Department of Chemistry.
[‡] Department of Physics and Astronomy.

10.1021/nl901232p CCC: $40.75
Published on Web 06/03/2009

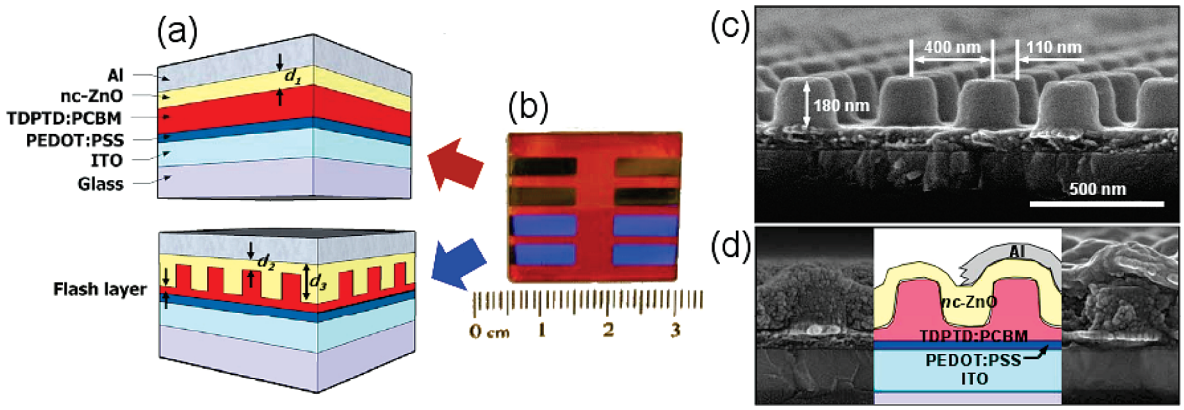

Figure 1. PC and planar geometries for organic solar cells. (a) Schematic of planar control (top) and PC (bottom) cells. (b) Planar cells (brown) and iridescent PC cells (blue) on the same device substrate. The angular dependent color from the PC cells derives from diffraction at large incident angles. (c) Scanning electron micrograph of hexagonal array of BHJ columns prior to backfilling with nc-ZnO. (d) Cross section of PC cell showing the hierarchical arrangement of components (left without Al overcoat), right (from the top): Al/nc-ZnO/patterned TDPTD:PCBM/Flash-layer TDPTD:PCBM/PEDOT:PSS/ITO/Glass.

improvements where both the fill factor (FF) and open circuit voltage (V_{oc}) are enhanced ~10%. The PC structure is formed in a single step by nanopatterning the photoactive BHJ blend, a relatively high refractive index material, into a hexagonal array of posts with 400 nm periodicity. The BHJ then interfaces with a transparent, low refractive index form of nanocrystalline zinc oxide (nc-ZnO), which provides enough optical contrast to enable PC behavior.

Figure 1 shows a schematic (a), photograph (b), and scanning electron micrograph (SEM) cross section (c,d) of PC solar cells. PC and planar cells are fabricated on the same device substrate and can be easily distinguished due to the bright iridescence of the PC device. Simultaneously fabricating PC and planar cells on the same substrate ensures that each contains an equivalent volume of photoactive material and undergoes identical fabrication steps and thermal history. In the PC cell, the photoactive TDPTD:PCBM constitutes both the planar flash layer (40 nm) and the hexagonal array of columnar features that are 180 nm in height (see Figure 1c). The TDPTD:PCBM mixture becomes insoluble after thermally curing[26] which enables control of the flash layer thickness in a spin-coating step prior to forming the PC geometry. A thin flash layer is critical in two respects: (1) it prevents direct contact between the nc-ZnO and the poly(3,4-ethylenedioxythiophene):poly(styrenesulfonate) (PEDOT:PSS) interface, and (2) it determines the height of the TDPTD:PCBM columns (the aspect ratio for equivalent flat-cell PV-active material contents), which in turn increases the photonic activity.

The nc-ZnO has been used in photovoltaic cells as an optical spacer,[27] an electron transport layer,[28] a high electron mobility film,[29] and an improved electrical contact for metal cathodes.[30] Herein the nc-ZnO serves as a refractive index contrast matrix in the PC cell and a "spacer layer" in the planar cell; it is formed by spin-coating a dispersion of freshly synthesized nc-ZnO[31] (~5 nm diameter particles) in methanol on both the embossed and planar photoactive strata (see Supporting Information for fabrication details). A cross section of the latter structure is shown in Figure 1d. Although an IR-vis-transparent material, the nc-ZnO layer can affect the absorption characteristics of the cell via interference effects,[27] so PC and planar cells with various nc-ZnO thicknesses were fabricated. Thus, in addition to controlling the thickness of the nc-ZnO layer in the planar cell (d_1), the thicknesses of the nc-ZnO film between and above the BHJ columns, d_2 and d_3, respectively, were varied (see Figure 1a). These values are given for five different sets of PC and planar cells fabricated on different device substrates in Table 1.

Table 1. Thicknesses of nc-ZnO for PC and Planar Cells Fabricated on Five Different Device Substrates

	nc-ZnO thickness (nm)	
device number	planar (d_1)	photonic crystal (d_2, d_3)
1	50	10, 30
2	90	40, 100
3	130	60, 150
4	200	70, 220
5	280	120, 300

Figure 2a shows the significant refractive index contrast of the optical properties of TDPTD:PCBM and nc-ZnO measured via spectroscopic ellipsometry. When combined with the 400 nm hexagonal periodicity of the PC, optimal conditions are met for band edge absorption enhancements in TDPTD:PCBM. Figure 2b shows the s-polarized zeroth order reflection measured at normal incidence for the PC and planar cells for device No. 2. (The p-polarization is nearly identical at normal incidence and is not shown.) Because of negligible transmission and scattering, (the iridescence effects are only appreciable at large incidence angles), the reflection (R) yields an approximation to the absorption (A) using $A = 100 - R$. Because of the ~90 nm active layer thickness of the planar cell, there is strong absorption in the visible range where the extinction coefficient of TDPTD:PCBM is high. This corresponds to essentially equivalent absorption in this wavelength range for PC and planar cells. However, for wavelengths longer than 600 nm, there is much stronger absorption in the PC cell as evidenced by the reduced reflection (Figure 2b). Specifically, the absorption is enhanced 3.5 times for the PC cell over the planar one for $\lambda = 660$ nm.

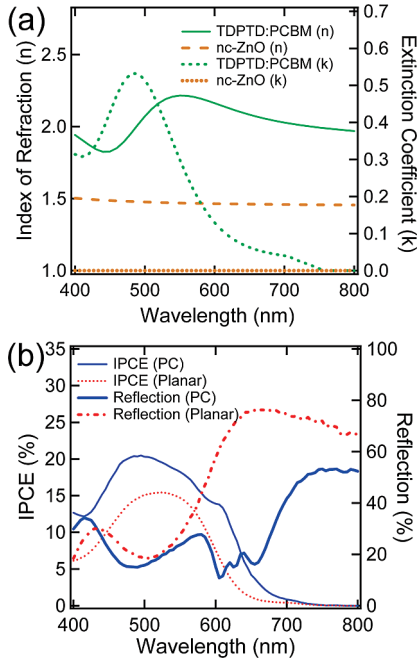

Figure 2. (a) Measured optical properties of the two materials that give the PC cell its high index of refraction contrast: the photoactive BHJ material, TDPTD:PCBM, and the transparent conductive oxide, nc-ZnO. (b) Zeroth order reflection and IPCE of PC and planar cells for s-polarized light at normal incidence for device No. 2.

Also shown in Figure 2b is the incident-photon-to-current conversion efficiency (IPCE) for the PC and planar cells. There is an enhancement for wavelengths where the PC cell is absorbing more strongly, but there is also an enhancement where they appear to have similar absorption in the visible range. A first step toward reconciling this effect requires a more precise determination of the absorption. The above-mentioned approximation of $A = 100 - R$ is a measure of the total absorption where losses in all internal layers are included. Even though PC and planar cells are fabricated on the same substrate and have equivalent volumes of all internal materials, the PC structure alters the optical profile in each internal layer due to its modulated thickness relative to the planar photoactive layer. This will cause changes in the optical field in layers that also absorb light but do not produce photocurrent, such as the indium tin oxide anode (ITO) and PEDOT:PSS. Thus, simply comparing the measured reflection only offers a first approximation to the photoactive absorption. Losses may be individually quantified by fitting a solution to Maxwell's equations to the measured reflection data. Once this is achieved, absorption in each layer is determined by calculating the change in the Poynting vector from interface to interface as is frequently done for planar devices.[32]

We construct an optical model using scattering matrix theory[33] which is a general form of the transfer matrix method commonly used to model planar organic solar cells.[27,32] The complex dielectric functions of the cell materials (TDPTD:PCBM and nc-ZnO shown in Figure 2a) are used as input in the model and were measured using spectroscopic ellipsometry (see Supporting Information for optical modeling details). The physical dimensions of the

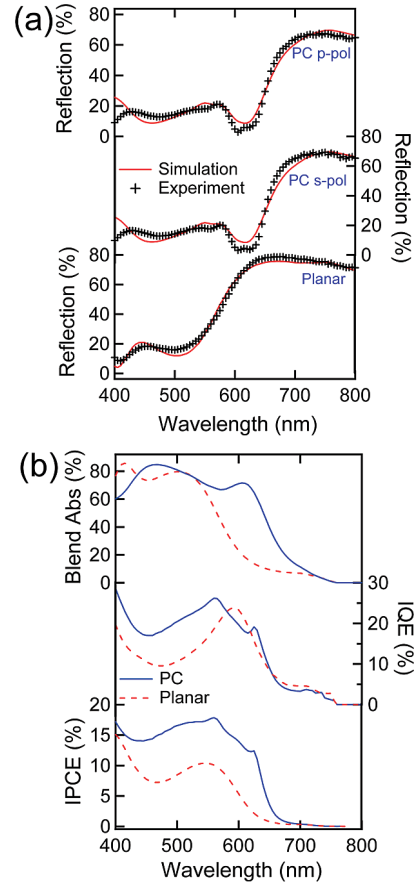

Figure 3. (a) Experimental and simulated zeroth order reflection for PC and planar cells for device No. 3 at normal incidence in both p- and s-polarization. The planar cell is equivalent in both polarizations. (b) Calculated TDPTD:PCBM absorption, IQE, and IPCE under s-polarized illumination.

device are then varied over a range close to measured SEM values until an appropriate fit with the experimental data is obtained. These results are given in Figure 3a for the PC and planar cells for device No. 3. Good agreement is obtained between the theory and experiment for both polarizations at normal incidence. The model is then used to calculate absorption in the TDPTD:PCBM blend that will yield photocurrent in the external circuit. Blend absorption is plotted for both PC and planar cells in Figure 3b for s-polarization. This is a different device with different nc-ZnO thicknesses from that presented in Figure 2b, but the tendency of enhanced absorption and IPCE is qualitatively identical. There is still essentially equivalent photoactive absorption in the visible range with an enhancement toward the band edge. Specifically, a 4.8-fold absorption enhancement is achieved at $\lambda = 630$ nm for the PC cell relative to the planar one. This contributes to an average tripling of absorption near the band edge ($580 \leq \lambda \leq 750$).

Applying the simulation method to our devices did yield an accurate measure of photoactive absorption, but it did not explain the enhanced IPCE in the visible range where absorption is essentially equivalent between PC and planar cells. By calculating absorption (ABS) in TDPTD:PCBM and measuring IPCE, we can calculate the internal quantum efficiency (IQE) by $\mathrm{IPCE}(\lambda) = \mathrm{IQE}(\lambda)\cdot\mathrm{ABS}(\lambda)$. The IQE is

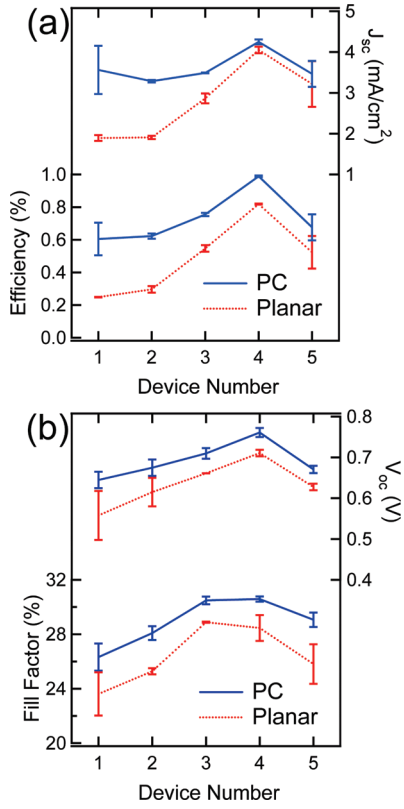

Figure 4. (a) Short circuit current (J_{sc}) and efficiency for PC and planar cells where comparisons are made between cells fabricated on the same device substrate. (b) The corresponding values of open circuit voltage (V_{oc}) and fill factor (FF). The mean values and error bars are an average over four cells per device.

a measure of the electrical processes in the cells at short circuit and is given for PC and planar device No. 3 in Figure 3b. Electrical processes include exciton dissociation at the BHJ donor/acceptor interface, drift and diffusion of free charge carriers through the blend, and carrier collection at the electrodes. As shown in Figure 3b, the IQE is enhanced in the visible spectral range, which indicates an inherent electrical enhancement for the PC cell.

In order to further investigate the electrical properties, device performance was evaluated in an inert atmosphere (purified nitrogen) under standard AM 1.5 testing conditions (see Figure S4 in Supporting Information for sample $I-V$ curve). The mean values of the short circuit current (J_{sc}), V_{oc}, FF, and efficiency are summarized in Figure 4 where comparisons are made between PC and planar cells fabricated on the same substrate according to Table 1. We observe an average enhancement over all devices (~20 cells for each geometry) of 10% for V_{oc} and 9% for FF for the PC devices. On the other hand, the J_{sc} shows more variable enhancements due to changes in optical absorption that result from optical interference. Overall, there is an average 68% efficiency enhancement for PC cells. We are currently investigating the improvement of the IQE, V_{oc}, and FF that are caused by the PC structure. As both planar and PC cells were fabricated simultaneously on the same device, both cell types were subjected to identical thermal processing. Hence we anticipate that the nanophase-separated BHJ morphology to be the same in both cells, that is, the internal blend interface

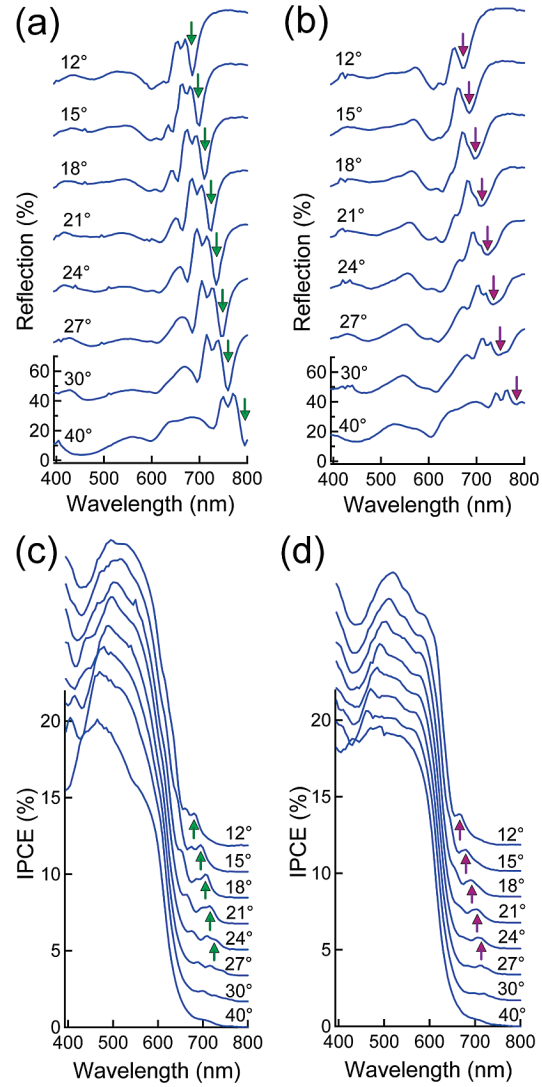

Figure 5. Angular dependent zeroth-order reflection and IPCE for PC cells for device No. 3. (a) p-polarized reflection, (b) s-polarized reflection, (c) p-polarized IPCE, and (d) s-polarized IPCE. The arrows denote sharp drops in reflection and corresponding increases in IPCE associated with resonant mode excitation.

where charge separation occurs should be identical in both cells. Calculations suggest that the PC topography generates a markedly different wavelength-dependent carrier creation profile compared to a planar cell and that may result in more favorable free carrier transport for TDPTD:PCBM.[19] This in turn, may be augmented by a 45% larger interface area between the blend and nc-ZnO in the PC cells. The conformal electrode on the PC topography may also alter the static internal electric field in the photoactive region that could change the field-dependent dissociation of excitons at the TDPTD-donor/PCBM-acceptor interface.[4]

Thus far we have described PC performance enhancements under normal light incidence. For non-normal illumination, resonant mode splitting occurs and generates absorption enhancements that exhibit a rich photonic behavior. This is demonstrated in Figure 5a−d for PC device No. 3 where the differences between p- and s-polarization can now be resolved in both reflection and IPCE measurements from 12 to 40°. Under normal incidence, resonant mode degeneracy

masks the actual number of modes excited in the PC geometry as indicated in the reflection data of Figures 2b and 3a. On the other hand, under non-normal conditions, three modes can be resolved in p-polarization with at least two modes in s-polarization near the band edge of TDPTD:PCBM. Enhancements in both polarizations are possible, because the PC geometry is periodic in both lateral dimensions. Arrows track the dispersion of the stronger modes along with the resulting IPCE enhancement. The spectral location of the band edge of TDPTD:PCBM is also apparent near $\lambda = 750$ nm, because the resonant modes as shown in reflection retain their shape even after they have red-shifted past the wavelength where TDPTD:PCBM becomes transparent and produces no photocurrent. These long wavelength excitations are possible because other strata in the cell such as PEDOT:PSS and ITO have nonzero extinction coefficients and absorb in the near-IR. Optical simulations confirm that ITO and PEDOT:PSS absorb a significant fraction of resonant mode energy for these incident angles even at wavelengths where photocurrent is produced (see Figure S3 in Supporting Information). This limits the observed photocurrent enhancement. Even so, along with the results for normal incidence, this demonstration of significant photonic activity should motivate further studies of BHJ materials with PC geometries that have greater intrinsic performance capabilities including low-bandgap polymer blends.

In summary, we have demonstrated the fabrication of BHJ organic solar cells with PC geometries. This has been achieved using the PRINT process where ordered arrays of submicrometer features can be made in a single step. The PC structure helps transcend the electrical performance constraints of a thin photoactive layer by boosting the FF and V_{oc}. Furthermore, it provides a method to target specifically desired regions of the solar spectrum for absorption enhancements via a photonic structure that exhibits multiple resonances.

Acknowledgment. Support for this work from NSF (NIRT: Bio-Inspired Actuating Structures CMS-0507151) and NASA (URETI Biologically Inspired Materials Grant NAG-1-2301) is gratefully acknowledged by D.-H.K. and E.T.S. J.R.T. and R.L. acknowledge support from the Army Research Office Grant W911NF-07-1-0539. We thank Robert Brady, Wei You, and Zhilian Zhou for stimulating conversations, Amar Kumbhar for help with TEM (CHANL, UNC-Chapel Hill), and Hong Gu Chun and Paul Hoertz for help with device measurements.

Supporting Information Available: Description of fabrication details, optical simulation method, and device measurement. This material is available free of charge via the Internet at http://pubs.acs.org.

References

(1) Halls, J. J. M.; Walsh, C. A.; Greenham, N. C.; Marseglia, E. A.; Friend, R. H.; Moratti, S. C.; Holmes, A. B. *Nature* **1995**, *376*, 498.
(2) Coakley, K. M.; McGehee, M. D. *Chem. Mater.* **2004**, *16*, 4533.
(3) Yu, G.; Gao, J.; Hummelen, J. C.; Wudl, F.; Heeger, A. J. *Science* **1995**, *270*, 1789.
(4) Mihailetchi, V. D.; Koster, L. J. A.; Hummelen, J. C.; Blom, P. W. M. *Phys. Rev. Lett.* **2004**, *93*, 216601.
(5) Scharber, M. C.; Mühlbacher, D.; Koppe, M.; Denk, P.; Waldauf, C.; Heeger, A. J.; Brabec, C. J. *Adv. Mater.* **2006**, *18*, 789.
(6) Moulé, A. J.; Meerholz, K. *Appl. Phys. B* **2007**, *86*, 721.
(7) Gunes, S.; Neugebauer, H.; Sariciftci, N. S. *Chem. Rev.* **2007**, *107*, 1324.
(8) Blom, P. W. M.; Mihailetchi, V. D.; Koster, L. J. A.; Markov, D. E. *Adv. Mater.* **2007**, *19*, 1551.
(9) Nunzi, J.-M. C. R. *Physique* **2002**, *3*, 523.
(10) Mühlbacher, D.; Scharber, M.; Morana, M.; Zhu, Z.; Waller, D.; Gaudiana, R.; Brabec, C. *Adv. Mater.* **2006**, *18*, 2884.
(11) Peumans, P.; Bulović, V.; Forrest, S. R.; Forrest, S. R. *Appl. Phys. Lett.* **2000**, *76*, 2650.
(12) Niggemann, M.; Glatthaar, M.; Lewer, P.; Müller, C.; Wagner, J.; Gombert, A. *Thin Solid Films* **2006**, *511−512*, 628.
(13) Rim, S.-B.; Zhao, S.; Scully, S. R.; McGehee, M. D.; Peumans, P. *Appl. Phys. Lett.* **2007**, *91*, 243501.
(14) Roman, L. S.; Inganäs, O.; Granlund, T.; Nyberg, T.; Svensson, M.; Andersson, M. R.; Hummelen, J. C. *Adv. Mater.* **2000**, *12*, 189.
(15) Niggemann, M.; Glatthaar, M.; Gombert, A.; Hinsch, A.; Wittwer, V. *Thin Solid Films* **2004**, *451−452*, 619.
(16) Na, S.-I.; Kim, S.-S.; Kwon, S.-S.; Jo, J.; Kim, J.; Lee, T.; Kim, D.-Y. *Appl. Phys. Lett.* **2007**, *91*, 173509.
(17) Duché, D.; Escoubas, L.; Simon, J.-J.; Torchio, P.; Vervisch, W.; Flory, F. *Appl. Phys. Lett.* **2008**, *92*, 193310.
(18) Tumbleston, J. R.; Ko, D.-H.; Samulski, E. T.; Lopez, R. *Appl. Phys. Lett.* **2009**, *94*, 043305.
(19) Tumbleston, J. R.; Ko, D.-H.; Samulski, E. T.; Lopez, R. *Opt. Express* **2009**, *17*, 7670.
(20) Bermel, P.; Luo, C.; Zeng, L.; Kimerling, L. C.; Joannopoulos, J. D. *Opt. Express* **2007**, *15*, 16986.
(21) Zhou, D.; Biswas, R. *J. Appl. Phys.* **2008**, *103*, 093102.
(22) Na, S.-I.; Kim, S.-S.; Jo, J.; Oh, S.-H.; Kim, J.; Kim, D.-Y. *Adv. Funct. Mater.* **2008**, *18*, 3956.
(23) Cocoyer, C.; Rocha, L.; Sicot, L.; Geffroy, B.; de Bettignies, R.; Sentein, C.; Fiorini-Debuisschert, C.; Raimond, P. *Appl. Phys. Lett.* **2006**, *88*, 133108.
(24) Kim, M.-S.; Kim, J.-S.; Cho, J. C.; Shtein, M.; Guo, L. J.; Kim, J. *Appl. Phys. Lett.* **2007**, *90*, 123113.
(25) Hampton, M. J.; Williams, S. S.; Zhou, Z.; Nunes, J.; Ko, D.-H.; Templeton, J. L.; Samulski, E. T.; DeSimone, J. M. *Adv. Mater.* **2008**, *20*, 2667.
(26) Liu, J.; Kadnikova, E. N.; Liu, Y.; McGehee, M. D.; Frechet, J. M. J. *J. Am. Chem. Soc.* **2004**, *126*, 9486.
(27) Gilot, J.; Barbu, I.; Wienk, M. M.; Janssen, R. A. J. *Appl. Phys. Lett.* **2007**, *91*, 113520.
(28) Gilot, J.; Wienk, M. M.; Janssen, R. A. J. *Appl. Phys. Lett.* **2007**, *90*, 143512.
(29) Roest, A. L.; Kelly, J. J.; Vanmaekelbergh, D.; Meulenkamp, E. A. *Phys. Rev. Lett.* **2002**, *89*, 036801.
(30) Yip, H.-L.; Hau, S. K.; Baek, N. S.; Ma, H.; Jen, A. K. Y. *Adv. Mater.* **2008**, *20*, 2376.
(31) Beek, W. J. E.; Wienk, M. M.; Kemerink, M.; Yang, X.; Janssen, R. A. J. *J. Phys. Chem. B* **2005**, *109*, 9505.
(32) Dennler, G.; Forberich, K.; Scharber, M. C.; Brabec, C. J.; Tomis, I.; Hingerl, K.; Fromherz, T. *J. Appl. Phys.* **2007**, *102*, 054516.
(33) Tikhodeev, S. G.; Yablonskii, A. L.; Muljarov, E. A.; Gippius, N. A.; Ishihara, T. *Phys. Rev. B* **2002**, *66*, 045102.

NL901232P